Cell-Free Massive MIMO-OFDM Transmission over Frequency-Selective Fading Channels

Wei Jiang, *Senior Member, IEEE,* and Hans Dieter Schotten, *Member, IEEE*

Abstract—This letter presents and analyzes orthogonal frequency-division multiplexing (OFDM)-based multi-carrier transmission for cell-free massive multi-input multi-output (CFmMIMO) over frequency-selective fading channels. Frequency-domain conjugate beamforming, pilot assignment, and user-specific resource allocation are proposed. The CFmMIMO-OFDM system is scalable to serve a massive number of users and is flexible to offer diverse data rates for heterogeneous applications.

Index Terms—Cell-free massive MIMO, cell edge, frequency-selective fading channel, massive MIMO-OFDM, OFDM.

I. INTRODUCTION

CELL-FREE massive multi-input multi-output (CFmMIMO) has recently received much attention from both academia and industry [1]. Different aspects of CFmMIMO such as resource allocation [2], power control [3], pilot assignment [4], energy efficiency [5], backhaul constraint [6], and scalability [7] have been studied. However, previous works merely considered frequency-flat fading (narrow-band) channels. Most of wireless communications nowadays are broadband with signal bandwidths far wider than the *coherence bandwidth*, leading to frequency selectivity. To the authors' best knowledge, only [8] discussed CFmMIMO over frequency-selective fading channels. But it applied single-carrier transmission that does not support high data rate due to prohibitively high complexity of signal equalization [9]. Moreover, the conventional CFmMIMO systems generally aim to offer uniform service by maximizing the minimum of per-user rate [3], whereas it neglects the fact that heterogeneous users have differentiated demands on data throughput.

To fill this gap, this letter will present and analyze orthogonal frequency-division multiplexing (OFDM)-based multi-carrier transmission for CFmMIMO, coined cell-free massive MIMO-OFDM (CFmMIMO-OFDM), over frequency-selective fading channels. Contamination-free pilot assignment and channel estimation in the uplink time-frequency grid, and *frequency-domain* conjugate beamforming in the downlink data transmission are provided. A user-specific resource allocation method that enables the scalability to accommodate massive number of users and the flexibility of offering diverse data rates is proposed. Per-user and sum data throughput, considering APs equipped with either single or multiple antennas,

TABLE I
DEFINITIONS OF MAIN MATHEMATICAL SYMBOLS.

Symbol	Definition
β_{mk}	Large-scale fading between AP antenna m and user k
$\mathbf{h}_{mk}$	Small-scale fading between AP antenna m and user k
$\mathbf{g}_{mk}$	Channel vector between AP antenna m and user k
$\mathbf{g}_{mk}^N$	N-point channel vector by padding zeros at the tail of $\mathbf{g}_{mk}$
$\tilde{\mathbf{g}}_{mk}$	Frequency-domain channel vector, i.e., the DFT of $\mathbf{g}_{mk}^N$
$\tilde{g}_{mk}^r$ and $\hat{g}_{mk}^r$	Frequency-domain channel response and its estimate
$\mathbf{x}_m$ and $\tilde{\mathbf{x}}_m$	Time- and frequency-domain transmitted symbol vectors
$\mathbf{x}_m^{cp}$ and $\mathbf{y}_k^{cp}$	Transmitted and received symbol vectors with cyclic prefix
$\mathbf{y}_k$ and $\tilde{\mathbf{y}}_k$	Time- and frequency-domain received symbol vectors
$\mathcal{U}$ and $\mathcal{U}_s$	The set of all users and the sth user group
$\mathbb{B}$ and $\mathbb{B}_s$	The set of all RBs and the RBs assigned to $\mathcal{U}_s$
K and K_r	The number of all users and the number of users over $\mathcal{B}_r$
N and N_{RB}	The number of subcarriers and the number of RBs

are evaluated. **Notations**:: Bold lower- and upper-case letters denote vectors and matrices, respectively, while $(\cdot)^*$, $(\cdot)^T$, and $(\cdot)^H$ express conjugate, transpose, and Hermitian transpose. For ease reference, main mathematical symbols and notation are listed in Table I.

II. SYSTEM MODEL

Consider a geographical area where M randomly distributed access points (APs) are connected to a central processing unit (CPU) via a fronthaul network and serve K users. We first assume that each AP and user is equipped with a single antenna as [1] for simple analysis but will demonstrate its adaptability to multi-antenna APs afterwards. In contrast to the conventional CFmMIMO such as [1]–[8] that requires $K \ll M$, the number of users in CFmMIMO-OFDM is scalable, ranging from small $K \ll M$ to very large $K \gg M$. Users are divided into groups and each group is assigned to different resource blocks (RBs). Thus, the constraint that the number of users is far smaller than M is still satisfied on each RB.

The previous works assume that the small-scale fading is frequency-flat, as modelled by a circularly-symmetric complex Gaussian random variable with zero mean and unit variance, i.e., $h[t] \sim \mathcal{CN}(0, 1)$. This assumption is only valid for narrow-band communications. Nevertheless, most of the current and future mobile communications [10] are broadband, suffering from severe frequency selectivity. This letter goes beyond the current state of the art by studying CFmMIMO over a frequency-selective fading channel [11]. It can be modeled as a linear time-varying filter $\mathbf{h}[t] = [h_0[t], \ldots, h_{L-1}[t]]^T$, where the filter length L should be no less than multi-path delay spread T_d normalized by the sampling interval T_s, namely $L \geqslant \left\lceil \frac{T_d}{T_s} \right\rceil$.
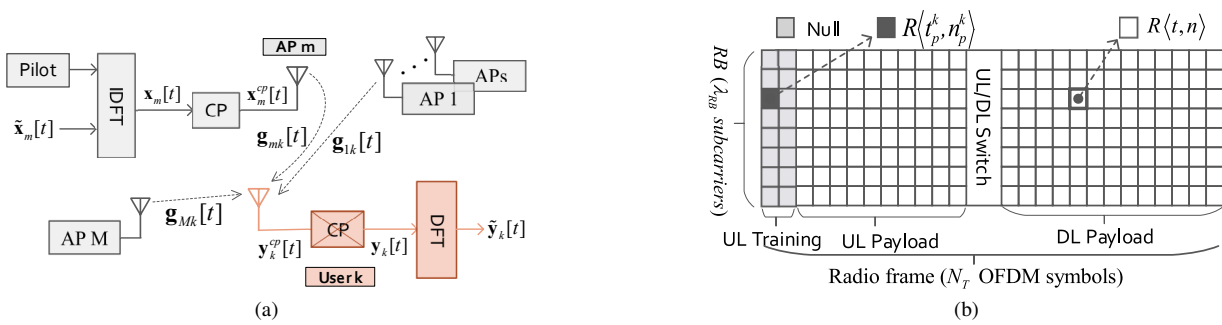
Fig. 1. Schematic diagram of a CFmMIMO-OFDM system where M AP antennas serve K users: Part (a) elaborates the OFDM transmitter at the mth AP antenna and the receiver at the kth user. A radio frame consists of N_T OFDM symbols in the axis of time and N subcarriers in the frequency domain, which are grouped into N_{RB} resource blocks. Part (b) illustrates the time-frequency resource grid of a single RB containing λ_{RB} consecutive subcarriers. UL/DL switch denotes the guard interval between the uplink and downlink transmission.

The tap gain $h_l[t] = \sum_i a_i(tT_s)e^{-j2\pi f_c \tau_i(tT_s)} sinc[l - \tau_i(tT_s)B_w]$ for $l = 0, \ldots, L - 1$, with carrier frequency f_c, attenuation $a_i(tT_s)$ and delay $\tau_i(tT_s)$ of the ith signal path, signal bandwidth $B_w = 1/T_s$, and $sinc(x) \triangleq \frac{\sin(x)}{x}$ for $x \neq 0$. The fading channel between AP m and user k is given by

$$\mathbf{g}_{mk}[t] = [g_{mk,0}[t], \ldots, g_{mk,L_{mk}-1}[t]]^T = \sqrt{\beta_{mk}[t]}\mathbf{h}_{mk}[t], \quad (1)$$

where $g_{mk,l}[t] = \sqrt{\beta_{mk}[t]}h_{mk,l}[t]$ and $\beta_{mk}[t]$ indicates large-scale fading, which is frequency independent and varies slowly.

III. Cell-Free Massive MIMO-OFDM system

The data transmission in an OFDM system [9] is organized in block-wise, as shown in Fig.1a. We write $\tilde{\mathbf{x}}_m[t] = [\tilde{x}_{m,0}[t], \ldots, \tilde{x}_{m,n}[t], \ldots, \tilde{x}_{m,N-1}[t]]^T$ to denote the frequency-domain transmission block of AP m on the tth OFDM symbol. (The tilde ~ marks frequency-domain variables throughout this letter.) Transform $\tilde{\mathbf{x}}_m[t]$ into a time-domain sequence $\mathbf{x}_m[t] = [x_{m,0}[t], \ldots, x_{m,n'}[t], \ldots, x_{m,N-1}[t]]^T$ through an N-point inverse discrete Fourier transform (IDFT), i.e., $x_{m,n'}[t] = \frac{1}{N}\sum_{n=0}^{N-1} \tilde{x}_{m,n}[t]e^{2\pi jn'n/N}$ for $n' = 0, 1, \ldots, N - 1$ and $j^2 = -1$. Defining the discrete Fourier transform (DFT) matrix

$$\mathbf{F} = \begin{bmatrix} \omega_N^{0\cdot0} & \cdots & \omega_N^{0\cdot(N-1)} \\ \vdots & \ddots & \vdots \\ \omega_N^{(N-1)\cdot0} & \cdots & \omega_N^{(N-1)\cdot(N-1)} \end{bmatrix} \quad (2)$$

with a primitive N^{th} root of unity $\omega_N^{n\cdot n'} = e^{2\pi jnn'/N}$, the OFDM modulation can be written in matrix form as

$$\mathbf{x}_m[t] = \mathbf{F}^{-1}\tilde{\mathbf{x}}_m[t] = \frac{1}{N}\mathbf{F}^*\tilde{\mathbf{x}}_m[t]. \quad (3)$$

A guard interval known as cyclic prefix (CP) is added between two consecutive blocks to avoid inter-symbol interference (ISI) and preserve orthogonality of subcarriers. Thus, we get $\mathbf{x}_m^{cp}[t] = [x_{m,N-L_{cp}}[t], \ldots, x_{m,N-1}[t], x_{m,0}[t], \ldots, x_{m,N-1}[t]]^T$ as the transmitted signal. The ISI can be eliminated if the length of CP is larger than the length of any channel filter, i.e., $L_{cp} > \max(L_{mk})$, for all $m \in \{1, \ldots, M\}$ and $k \in \{1, \ldots, K\}$.

The signal $\mathbf{x}_m^{cp}[t]$ goes through the channel $\mathbf{g}_{mk}[t]$ to reach the typical user k, resulting in $\mathbf{x}_m^{cp}[t] \star \mathbf{g}_{mk}[t]$, where $\star$ denotes *the linear convolution*. Thus, the overall received signal at user

k is $\mathbf{y}_k^{cp}[t] = \sum_{m=1}^{M} \mathbf{x}_m^{cp}[t] \star \mathbf{g}_{mk}[t] + \mathbf{z}_k[t]$, where $\mathbf{z}_k[t]$ is a vector of additive noise. Removing the CP, we get

$$\mathbf{y}_k[t] = \sum_{m=1}^{M} \mathbf{g}_{mk}^N[t] \otimes \mathbf{x}_m[t] + \mathbf{z}_k[t], \quad (4)$$

where $\otimes$ stands for *the cyclic convolution* [9] and $\mathbf{g}_{mk}^N[t]$ is an N-point channel filter formed by padding zeros at the tail of $\mathbf{g}_{mk}[t]$, i.e., $\mathbf{g}_{mk}^N[t] = [g_{mk,0}[t], \ldots, g_{mk,L_{mk}-1}[t], 0, \ldots, 0]^T$. The DFT demodulator outputs

$$\tilde{\mathbf{y}}_k[t] = \mathbf{F}\mathbf{y}_k[t]. \quad (5)$$

Substituting (3) and (4) into (5), and applying *the convolution theorem* for DFT [9], we have

$$\tilde{\mathbf{y}}_k[t] = \sum_{m=1}^{M} \mathbf{F}\left(\mathbf{g}_{mk}^N[t] \otimes \mathbf{x}_m[t]\right) + \mathbf{F}\mathbf{z}_k[t]$$
$$= \sum_{m=1}^{M} \tilde{\mathbf{g}}_{mk}[t] \odot \tilde{\mathbf{x}}_m[t] + \tilde{\mathbf{z}}_k[t], \quad (6)$$

where $\odot$ represents the Hadamard product (element-wise multiplication), $\tilde{\mathbf{g}}_{mk}[t] = \mathbf{F}\mathbf{g}_{mk}^N[t]$ and $\tilde{\mathbf{z}}_k[t] = \mathbf{F}\mathbf{z}_k[t]$ denote frequency-domain channel response and noise, respectively. At last a frequency-selective channel is transformed into a set of N independent frequency-flat subcarriers. The signal transmission in the downlink on the nth subcarrier is given by

$$\tilde{y}_{k,n}[t] = \sum_{m=1}^{M} \tilde{g}_{mk,n}[t]\tilde{x}_{m,n}[t] + \tilde{z}_{k,n}[t], \quad k \in \{1, \ldots, K\}, \quad (7)$$

where $\tilde{g}_{mk,n}[t]$ is the nth element of $\tilde{\mathbf{g}}_{mk}[t]$. Similarly, the uplink transmission is expressed by

$$\tilde{y}_{m,n}[t] = \sum_{k=1}^{K} \tilde{g}_{mk,n}[t]\tilde{x}_{k,n}[t] + \tilde{z}_{m,n}[t], \quad m \in \{1, \ldots, M\}. \quad (8)$$

IV. The communication process

The downlink (DL) transmission from the APs to the users and the uplink (UL) from the users to the APs are separated by time-division multiplexing (TDD) with the assumption of perfect channel reciprocity. A radio frame is mainly divided into three phases: UL training, UL payload transmission, and DL payload transmission.

A. Uplink Training

We write $\mathscr{R}\langle t,n\rangle$ to denote a resource unit (RU) on the nth subcarrier of the tth OFDM symbol. The time-frequency resource of a radio frame is divided into N_{RB} RBs, each of which contains $\lambda_{RB} = N/N_{RB}$ (assumed to be an integer) consecutive subcarriers. The rth RB is defined as $\mathcal{B}_r \triangleq \{\mathscr{R}\langle t,n\rangle | 1 \le t \le N_T \text{ and } (r-1)\lambda_{RB} \le n < r\lambda_{RB}\}$, for any $r \in \{1,\ldots,N_{RB}\}$, as illustrated in Fig.1b. The transmission of a radio frame in CFmMIMO is carried out within the *coherent time* and the width of one RB is smaller than the *coherence bandwidth*. Consequently, this letter simply adopts the *block fading* model where the channel coefficients for all RUs within one RB are assumed to be identical, we have

$$\tilde{g}_{mk,n}[t] = \tilde{g}_{mk}^r \impliedby \mathscr{R}\langle t,n\rangle \in \mathcal{B}_r. \qquad (9)$$

The channel estimation of a conventional CFmMIMO system relies on time-domain pilot sequences, where the maximal number of orthogonal sequences is τ_p by using τ_p pilot symbols. If $K \le \tau_p$ as assumed in [3], pilot contamination can be avoided. Owing to the limitation of the frame length, however, some users need to share the same sequence when $K > \tau_p$, leading to pilot contamination [4]. In contrast, CFmMIMO-OFDM is able to provide more orthogonal pilots by means of frequency-division multiplexing thanks to the extra degree of freedom gained from the frequency domain. To estimate $\tilde{g}_{mk}^r$, each user on $\mathcal{B}_r$ needs only one pilot symbol. Suppose the first τ_p OFDM symbols are dedicated to the uplink training, one RB has $N_p = \tau_p\lambda_{RB}$ orthogonal pilots. The number of users allocated to $\mathcal{B}_r$ is denoted by K_r, there is no pilot contamination if $K_r \le N_p$, which is a very relaxed condition. We write $\mathscr{R}\langle t_p^k, n_p^k\rangle$ with $1 \le t_p^k \le \tau_p$ and $(r-1)\lambda_{RB} \le n_p^k < r\lambda_{RB}$ to denote the RU reserved for the pilot symbol of user k, $k \in \{1,\ldots,K_r\}$. Other users keep silence (null) on this RU to achieve orthogonality. As illustrated in Fig.1b, the pilot assignment is specified by

$$\tilde{x}_{k,n}[t] = \begin{cases} \sqrt{p_u}\,\mathbb{P}_k, & \text{if } t = t_p^k \wedge n = n_p^k \\ 0, & \text{otherwise} \end{cases}, \quad 1 \le t \le \tau_p, \quad (10)$$

where $\wedge$ represents logical AND, $\mathbb{P}_k$ is the known pilot symbol with $\mathbb{E}[|\mathbb{P}_k|^2] = 1$, and p_u denotes the UL transmit power limit.

Substituting (9) and (10) into (8), we get the received signal of the mth AP on $\mathscr{R}\langle t_p^k, n_p^k\rangle$ as

$$\tilde{y}_{m,n_p^k}[t_p^k] = \sum_{k=1}^{K_r} \tilde{g}_{mk,n_p^k}[t_p^k]\tilde{x}_{k,n_p^k}[t_p^k] + \tilde{z}_{m,n_p^k}[t_p^k]$$

$$= \tilde{g}_{mk,n_p^k}[t_p^k]\tilde{x}_{k,n_p^k}[t_p^k] + \sum_{k'\neq k}^{K_r} \tilde{g}_{mk',n_p^k}[t_p^k]\tilde{x}_{k',n_p^k}[t_p^k] + \tilde{z}_{m,n_p^k}[t_p^k]$$

$$= \sqrt{p_u}\tilde{g}_{mk,n_p^k}[t_p^k]\mathbb{P}_k + \tilde{z}_{m,n_p^k}[t_p^k]$$

$$= \sqrt{p_u}\tilde{g}_{mk}^r\mathbb{P}_k + \tilde{z}_{m,n_p^k}[t_p^k]. \qquad (11)$$

Let $\hat{g}_{mk}^r$ be an estimate of $\tilde{g}_{mk}^r$, we have $\hat{g}_{mk}^r = \tilde{g}_{mk}^r - \xi_{mk}^r$ with estimation error ξ_{mk}^r raised by additive noise. Applying the minimum mean-square error (MMSE) estimation gets

$$\hat{g}_{mk}^r = \left(\frac{R_{gg}\mathbb{P}_k^*}{R_{gg}|\mathbb{P}_k|^2 + R_{nn}}\right)\tilde{y}_{m,n_p^k}[t_p^k] = \left(\frac{\beta_{mk}\mathbb{P}_k^*}{\beta_{mk}|\mathbb{P}_k|^2 + \sigma_z^2}\right)\tilde{y}_{m,n_p^k}[t_p^k], \qquad (12)$$

which applies $R_{gg} = \mathbb{E}\left[|\tilde{g}_{mk}^r|^2\right] = \beta_{mk}$ and $R_{nn} = \mathbb{E}\left[|\tilde{z}_{m,n}[t]|^2\right] = \sigma_z^2$. Compute the variance of $\hat{g}_{mk}^r$ as

$$\mathbb{E}\left[\hat{g}_{mk}^r(\hat{g}_{mk}^r)^*\right] = \mathbb{E}\left[\frac{\beta_{mk}^2 |\mathbb{P}_k|^2 \left|\sqrt{p_u}\tilde{g}_{mk}^r\mathbb{P}_k + \tilde{z}_{m,n_p^k}[t_p^k]\right|^2}{(\beta_{mk}|\mathbb{P}_k|^2 + \sigma_z^2)^2}\right]$$

$$= \frac{\beta_{mk}^2 \mathbb{E}\left[\left|\sqrt{p_u}\tilde{g}_{mk}^r\mathbb{P}_k + \tilde{z}_{m,n_p^k}[t_p^k]\right|^2\right]}{(\beta_{mk} + \sigma_z^2)^2} = \frac{p_u\beta_{mk}^2}{p_u\beta_{mk} + \sigma_z^2}.$$

Consequently, we know that $\hat{g}_{mk}^r \in \mathcal{CN}(0, \alpha_{mk})$ with $\alpha_{mk} = \frac{p_u\beta_{mk}^2}{p_u\beta_{mk}+\sigma_z^2}$, in comparison with $\tilde{g}_{mk}^r \in \mathcal{CN}(0,\beta_{mk})$.

B. Uplink Payload Data Transmission

Suppose τ_u OFDM symbols are used for uplink transmission, on the RU $\mathscr{R}\langle t,n\rangle \in \mathcal{B}_r$, $\tau_p < t \le \tau_p + \tau_u$, all K_r users simultaneously transmit their signals to the APs. The kth user weights its transmit symbol $q_{k,n}[t]$, $\mathbb{E}\left[|q_{k,n}[t]|^2\right] = 1$, by a power-control coefficient $\sqrt{\psi_k}$, $0 \le \psi_k \le 1$. Substituting $\tilde{x}_{k,n}[t] = \sqrt{\psi_k p_u}q_{k,n}[t]$ into (8) yields

$$\tilde{y}_{m,n}[t] = \sqrt{p_u}\sum_{k=1}^{K_r} \tilde{g}_{mk,n}[t]\sqrt{\psi_k}q_{k,n}[t] + \tilde{z}_{m,n}[t]. \qquad (13)$$

C. Downlink Payload Data Transmission

Inspired by [1]–[5] that apply conjugate beamforming in the downlink, CFmMIMO-OFDM employs conjugate beamforming in the frequency domain. On $\mathscr{R}\langle t,n\rangle \in \mathcal{B}_r$, $\tau_p+\tau_u < t \le N_T$, each AP multiplexes a total of K_r symbols, i.e., $s_{k,n}[t]$ intended to user k, $k = 1,\ldots,K_r$, before transmission. With a power-control coefficient $\sqrt{\eta_{mk}}$, $0 \le \eta_{mk} \le 1$, the transmitted signal of the mth AP is

$$\tilde{x}_{m,n}[t] = \sqrt{p_d}\sum_{k=1}^{K_r} \sqrt{\eta_{mk}}(\hat{g}_{mk,n}[t])^* s_{k,n}[t]. \qquad (14)$$

Substituting (14) into (7) to get the received signal at user k

$$\tilde{y}_{k,n}[t] = \sqrt{p_d}\sum_{m=1}^{M} \tilde{g}_{mk,n}[t]\sum_{k'=1}^{K_r} \sqrt{\eta_{mk'}}(\hat{g}_{mk',n}[t])^* s_{k',n}[t] + \tilde{z}_{k,n}[t]$$

$$= \underbrace{\sqrt{p_d}\sum_{m=1}^{M} \sqrt{\eta_{mk}}|\hat{g}_{mk,n}[t]|^2 s_{k,n}[t]}_{Desired\ Signal}$$

$$+ \underbrace{\sqrt{p_d}\sum_{m=1}^{M} \hat{g}_{mk,n}[t]\sum_{k'\neq k}^{K_r} \sqrt{\eta_{mk'}}(\hat{g}_{mk',n}[t])^* s_{k',n}[t]}_{Multi-User\ Interference} \qquad (15)$$

$$+ \underbrace{\sqrt{p_d}\sum_{m=1}^{M} \xi_{mk,n}[t]\sum_{k'=1}^{K_r} \sqrt{\eta_{mk'}}(\hat{g}_{mk',n}[t])^* s_{k',n}[t]}_{Channel-Estimate\ Error} + \underbrace{\tilde{z}_{k,n}[t]}_{Noise}.$$

Each user is assumed to have the knowledge of channel statistics $\mathbb{E}\left[\sum_{m=1}^{M} \sqrt{\eta_{mk}}|\hat{g}_{mk,n}[t]|^2\right]$ rather than channel realizations $\hat{g}_{mk,n}[t]$ since there is no pilot and channel estimation in the downlink. Applying a similar method used in *Theorem 1* of

[1], we can derive that the spectral efficiency of user k on $\mathscr{R}\langle t, n \rangle \in \mathcal{B}_r$ is lower bounded by $\log_2\left(1 + \gamma_k^{\langle t,n \rangle}\right)$ with

$$\gamma_k^{\langle t,n \rangle} = \frac{p_d \left(\sum_{m=1}^{M} \sqrt{\eta_{mk}} \alpha_{mk}\right)^2}{\sigma_z^2 + p_d \sum_{m=1}^{M} \beta_{mk} \sum_{k'=1}^{K_r} \eta_{mk'} \alpha_{mk'}}, \qquad (16)$$

implying that the effect of small-scale fading is vanished (a.k.a. channel hardening), such that $\gamma_k^{\langle t,n \rangle} = \gamma_k^r$, for all $\mathscr{R}\langle t, n \rangle \in \mathcal{B}_r$.

V. USER-SPECIFIC RESOURCE ALLOCATION

The conventional CFmMIMO systems [1]–[8] can support only very few $K \ll M$ users with uniform quality of service. By exploiting the frequency domain, CFmMIMO-OFDM is adaptive to different numbers of users from a few $K \ll M$ to massive $K \gg M$ and is flexible to offer diverse data rates for heterogeneous users. Classify all users $\mathscr{U} = \{u_1, u_2, \cdots, u_K\}$ into different groups $\mathscr{U}_s$, $s = 1, 2, \ldots, S$ in terms of their demands on data throughput, subjecting to $\bigcup_{s=1}^{S} \mathscr{U}_s = \mathscr{U}$ and $\mathscr{U}_s \cap \mathscr{U}_{s'} = \varnothing$, $\forall s' \neq s$. The number of users in $\mathscr{U}_s$ satisfies $|\mathscr{U}_s| \ll M$ and $\sum_{s=1}^{S} |\mathscr{U}_s| = K$, where $|\cdot|$ stands for the cardinality of a set. The resource pool is $\mathbb{B} = \{\mathcal{B}_r | 1 \leq r \leq N_{RB}\}$ where the granularity for allocation is one RB. Using $\mathbb{B}_s$ to denote the RBs allocated to $\mathscr{U}_s$, we have $\bigcup_{s=1}^{S} \mathbb{B}_s \in \mathbb{B}$ (when all RBs are used, $\bigcup_{s=1}^{S} \mathbb{B}_s = \mathbb{B}$) and $\mathbb{B}_s \cap \mathbb{B}_{s'} = \varnothing$, $\forall s' \neq s$. If $\mathcal{B}_r \in \mathbb{B}_s$, the number of users served by this RB is $K_r = |\mathscr{U}_s|$. For any user $k \in \mathscr{U}_s$, its per-user data rate in the downlink is

$$R_k = \left(1 - \frac{\tau_p + \tau_u}{N_T}\right) \sum_{\mathcal{B}_r \in \mathbb{B}_s} \lambda_{RB} \triangle f \log_2\left(1 + \gamma_k^r\right), \qquad (17)$$

where $\triangle f$ is the subcarrier spacing. Then, the downlink sum data throughput of the system is $R_d = \sum_{s=1}^{S} \sum_{k \in \mathscr{U}_s} R_k$.

VI. ADAPTABILITY TO MULTI-ANTENNA AP

Inspired by [12], which argues that channel hardening and favorable propagation can be more easily obtained by deploying multiple antennas per AP, we further study CFmMIMO-OFDM with multi-antenna APs [5]. Generalizing the number of antennas per AP to $N_t \geqslant 1$, there are $N_{AP} = M/N_t$ (assumed to be an integer) homogeneous APs indexed by $q = 1, \ldots, N_{AP}$. The only difference raised by multi-antenna APs is that collocated antennas have identical large-scale fading, i.e., $\beta_{mk} = \beta_{qk}$ for any $m = (q-1)N_t + 1, \ldots, qN_t$. As [5] and [12], small-scale fading from each collocated antenna to the typical user is assumed to be independent. As a result, the channel model with multi-antenna APs is simply a special case of $\mathbf{g}_{mk}$ in (1), which is transparent to the communication process and does not need any modifications. When the users transmit pilot symbols, see (11), the observation at AP q is

$$\tilde{\mathbf{y}}_{q,n_p^k}[t_p^k] = \sqrt{p_u} \tilde{\mathbf{g}}_{qk}^r \mathbb{P}_k + \tilde{\mathbf{z}}_{q,n_p^k}[t_p^k],$$

where $\tilde{\mathbf{y}}_q$ and $\tilde{\mathbf{z}}_q$ are $N_t \times 1$ received symbol and noise vectors, respectively, and $\tilde{\mathbf{g}}_{qk}^r = \left[\tilde{g}_{(q-1)N_t+1,k}^r, \ldots, \tilde{g}_{qN_t,k}^r\right]^T \in \mathcal{C}^{N_t \times 1}$ stands for the channel vector between AP q and user k. Similar to (12), the MMSE estimate of $\tilde{\mathbf{g}}_{qk}^r$ can be obtained by

$$\hat{\mathbf{g}}_{qk}^r = \left(\frac{\mathbf{R}_{gg} \mathbb{P}_k^*}{\mathbf{R}_{gg} |\mathbb{P}_k|^2 + \mathbf{R}_{nn}}\right) \tilde{\mathbf{y}}_{q,n_p^k}[t_p^k] = \left(\frac{\beta_{qk} \mathbb{P}_k^*}{\beta_{qk} |\mathbb{P}_k|^2 + \sigma_z^2}\right) \tilde{\mathbf{y}}_{q,n_p^k}[t_p^k], \qquad (18)$$

which applies $\mathbf{R}_{gg} = \beta_{qk} \mathbf{I}_{N_t}$ and $\mathbf{R}_{nn} = \sigma_z^2 \mathbf{I}_{N_t}$, and we get $\hat{\mathbf{g}}_{qk}^r \in \mathcal{CN}(\mathbf{0}, \alpha_{qk} \mathbf{I}_{N_t})$ with $\alpha_{qk} = \frac{p_u \beta_{qk}^2}{p_u \beta_{qk} + \sigma_z^2}$. The transmitted signal can also be expressed by (14) since each antenna independently generates its signal using local channel estimates, regardless of how many antennas per AP. With conjugate beamforming, the power control is generally decided by β_{qk} [3], we have $\eta_{mk} = \eta_{qk}$ for $m = (q-1)N_t + 1, \ldots, qN_t$. Then, (16) can be rewritten for the case of multi-antenna AP as

$$\gamma_k^{\langle t,n \rangle} = \frac{p_d N_t^2 \left(\sum_{q=1}^{N_{AP}} \sqrt{\eta_{qk}} \alpha_{qk}\right)^2}{\sigma_z^2 + p_d N_t \sum_{q=1}^{N_{AP}} \beta_{qk} \sum_{k'=1}^{K_r} \eta_{qk'} \alpha_{qk'}}. \qquad (19)$$

VII. NUMERICAL RESULTS

The performance of CFmMIMO-OFDM in terms of per-user and sum rates is evaluated. We consider a square area of $1 \times 1 \text{km}^2$ where a total of M AP antennas serve K users. The COST-Hata model in [1] is applied for the path loss, where the three-slope breakpoints take values $d_0 = 10\text{m}$ and $d_1 = 50\text{m}$ while $L = 140.72\text{dB}$ with carrier frequency $f_c = 1.9\text{GHz}$, the height of AP antenna $h_{AP} = 15\text{m}$, and the height of user antenna $h_u = 1.65\text{m}$. Use $\beta_{mk} = 10^{\frac{PL_{mk}+X_{mk}}{10}}$ to get large-scale fading, where the shadowing fading $X_{mk} \sim \mathcal{N}(0, \sigma_{sd}^2)$ with $\sigma_{sd} = 8\text{dB}$. 3GPP Extended Typical Urban (ETU) model specified by delay profile in millisecond of $\{0, 0.05, 0.12, 0.2, 0.23, 0.5, 1.6, 2.3, 5\}$ with relative power as $\{-1, -1, -1, 0, 0, 0, -3, -5, -7\}$ is applied for small-scale fading[1]. The maximum transmit power of AP antenna and user are $p_d = 0.2\text{W}$ and $p_u = 0.1\text{W}$, respectively. The APs simply adopt the full-power transmission strategy, i.e., $\eta_{mk} = \left(\sum_{k=1}^{K_r} \alpha_{mk}\right)^{-1}$. The white noise power density is -174dBm/Hz with a noise figure of 9dB. Deducting a guard band of 1MHz at both sides, the signal bandwidth of $B_w = 20\text{MHz}$ is divided into $N = 1200$ subcarriers with $\triangle f = 15\text{kHz}$. Each RB consists of $\lambda_{RB} = 12$ subcarriers and thus $N_{RB} = 100$. We apply $N_T = 10$ for a frame including τ_p pilot symbols and $N_T - \tau_p$ downlink symbols, neglecting uplink transmission (i.e., $\tau_u = 0$) in our simulation.

Fig.2a compares cumulative distribution functions (CDFs) of per-user and sum rates over a single RB (i.e., 180kHz) achieved by CFmMIMO-OFDM with $M = 128$ single-antenna APs and $K_r = 6$, 12, 24, or 36. As we expected, per-user rate decreases when more users share the same amount of resource. But the more users are served together, the higher sum data throughput is achieved. In contrast to a single RB, the system can offer diverse transmission rates through the user-specific resource allocation. Table II shows the achievable capacity of the whole system using 100 RBs. We are interested in two extreme cases: mobile broadband (MBB) that requires very high rate and machine-type communications (MTC) with a massive number of low-rate users. Let $K = 6$ MBB users (only

---

[1]The near-far effect raised by distributed APs not only generates different distance-dependent large-scale fading but also causes diverse delay spreads in small-scale fading. Due to channel hardening, however, small-scale fading does not affect the final performance of conjugate beamforming, which relies only on large-scale fading. This argument can be proved by (16) and (19), and is observed also in simulations. However, it is necessary to consider heterogeneous delay spreads raised by cell free anywhere small-scale fading can affect performance.

TABLE II
95%-LIKELY AND 50%-LIKELY (MEDIAN) PER-USER DATA RATES, AND AVERAGED SUM DATA THROUGHPUT FOR MBB AND MTC.

System / Rate	$M = 128$							$M = 256$		$M = 512$	
	MBB				MTC			MBB	MTC	MBB	MTC
	$K = 6$	$K = 12$	$K = 24$	$K = 36$	$K = 1200$	$K = 2400$	$K = 3600$	$K = 6$	$K = 3600$	$K = 6$	$K = 3600$
95%-likely [Mbps]	28.20	19.96	10.34	5.66	0.199	0.103	0.057	40.47	0.137	54.40	0.229
Median [Mbps]	46.45	38.19	27.64	20.61	0.381	0.276	0.206	59.55	0.297	74.16	0.401
Sum [Mbps]	273.70	448.21	644.92	720.70	447.83	644.50	721.23	351.57	1034.97	437.44	1397.28
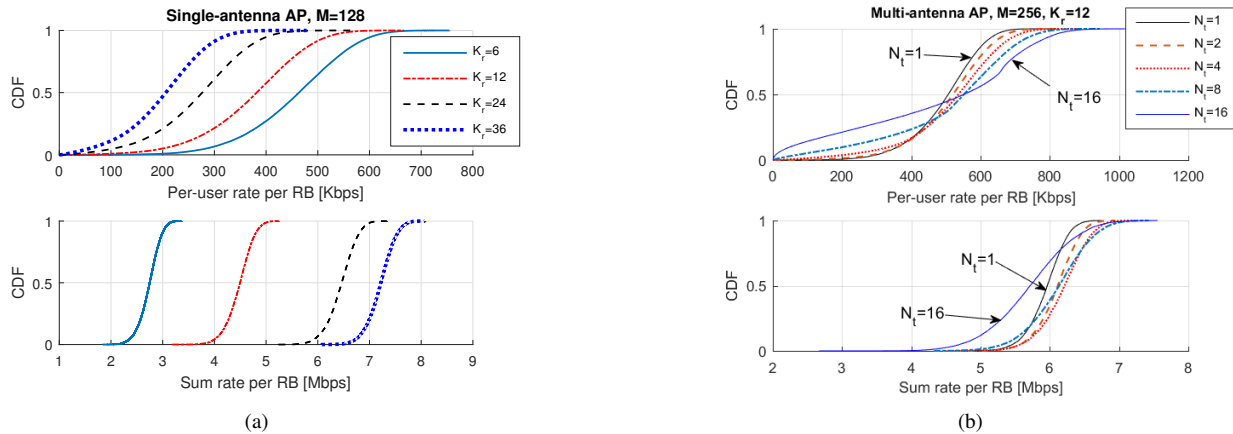
Fig. 2. Performance comparison with respect to the CDFs of per-user and sum data rates over a single RB. Part (a) utilizes $M = 128$ *single-antenna* APs and the number of users varies from $K_r = 6$, 12, 24, to 36. In part (b), a total of $M = 256$ antennas are distributed over a set of *multi-antenna* APs (with $N_t = 1$, 2, 4, 8 or 16) to serve $K_r = 12$ users.

one group) consume all 100 RBs, the 95%-likely per-user rate can reach 28.2Mbps and the 50%-likely or median rate is 46.45Mbps with $M = 128$. Increased to $M = 512$, an MBB user can get a 95%-likely rate of 54.4Mbps and a median rate of 74.16Mbps. In contrast, we equally divide $K = 3600$ users into $S = 100$ groups to accommodate as many MTC users as possible. Each group with $K_r = 36$ users is allocated with a single RB. With $M = 128$, each MTC user gets a 95%-likely rate of 57Kbps and a median rate of 206Kbps. Using $M = 512$, the system can support 3600 MTC users with an experienced rate of 229Kbps. In addition, the performance of multi-antenna APs is also evaluated where a total of $M = 256$ antennas serve $K_r = 12$ users. When the number of antennas per AP increases from $N_t = 1$ to 2, both per-user and sum rates boost, as shown in Fig.2b. Increased to $N_t = 4$, although the sum rate can grow slightly, the 95%-likely per-user rate drops. Remarkable performance loss on both per-user and sum rates is observed if $N_t = 16$. That is because some users may locate far away from any APs when there are only a few APs, implying the Marco-diversity stemming from CFmMIMO vanishes.

VIII. CONCLUSION

The proposed CFmMIMO-OFDM system is effective to combat frequency selectivity and pilot contamination can be eliminated by exploiting frequency-domain orthogonal pilots. In contrast to CFmMIMO that supports only very few users with uniform service quality, it is scalable to the scale of users and is adaptive to diverse service demands. It was verified by numerical results that CFmMIMO-OFDM can accommodate different numbers of users ranging from a few to thousands and can offer data rates from tens of Kbps to tens of Mbps.

REFERENCES

[1] H. Q. Ngo *et al.*, "Cell-free massive MIMO versus small cells," *IEEE Trans. Wireless Commun.*, vol. 16, no. 3, pp. 1834–1850, Mar. 2017.
[2] S. Buzzi *et al.*, "User-centric 5G cellular networks: Resource allocation and comparison with the cell-free massive MIMO approach," *IEEE Trans. Wireless Commun.*, vol. 19, no. 2, pp. 1250–1264, Feb. 2020.
[3] E. Nayebi *et al.*, "Precoding and power optimization in cell-free massive MIMO systems," *IEEE Trans. Wireless Commun.*, vol. 16, no. 7, pp. 4445–4459, Jul. 2017.
[4] W. Zeng *et al.*, "Pilot assignment for cell-free massive MIMO systems using a weighted graphic framework," *IEEE Trans. Veh. Technol.*, Apr. 2021, doi:10.1109/TVT.2021.3076440.
[5] H. Q. Ngo *et al.*, "On the total energy efficiency of cell-free massive MIMO," *IEEE Trans. Green Commun. Netw.*, vol. 2, no. 1, pp. 25–39, Mar. 2018.
[6] H. Masoumi and M. J. Emadi, "Performance analysis of cell-free massive MIMO system with limited fronthaul capacity and hardware impairments," *IEEE Trans. Wireless Commun.*, vol. 19, no. 2, pp. 1038–1052, Feb. 2020.
[7] E. Björnson and L. Sanguinetti, "Scalable cell-free massive MIMO systems," *IEEE Trans. Commun.*, vol. 68, no. 7, pp. 4247–4261, Jul. 2020.
[8] S.-N. Jin, D.-W. Yue, and H. H. Nguyen, "Spectral efficiency of a frequency-selective cell-free massive MIMO system with phase noise," *IEEE Wireless Commun. Lett.*, Dec. 2020.
[9] W. Jiang and T. Kaiser, "From OFDM to FBMC: Principles and Comparisons," in *Signal Processing for 5G: Algorithms and Implementations*, F. L. Luo and C. Zhang, Eds. United Kindom: John Wiley&Sons and IEEE Press, 2016, ch. 3.
[10] W. Jiang *et al.*, "The road towards 6G: A comprehensive survey," *IEEE Open J. Commun. Society*, vol. 2, pp. 334–366, Feb. 2021.
[11] D. Tse and P. Viswanath, *Fundamentals of Wireless Communication*. Cambridge, UK: Cambridge Univ. Press, 2005, ch. 2.
[12] Z. Chen and E. Björnson, "Channel hardening and favorable propagation in cell-free massive MIMO with stochastic geometry," *IEEE Trans. Commun.*, vol. 66, no. 11, pp. 5205–5219, Nov. 2018.